TECTONICS, VOL. 32, 501–515, doi:10.1002/tect.20042, 2013

Quaternary deformation along the Meeman-Shelby Fault near Memphis, Tennessee, imaged by high-resolution marine and land seismic reflection profiles

Yanjun Hao,[1] Maria Beatrice Magnani,[1] Kirk McIntosh,[2] Brian Waldron,[3] and Lei Guo[1]

Received 17 December 2012; revised 3 April 2013; accepted 9 April 2013; published 30 May 2013.

[1] A series of high-resolution seismic reflection surveys was carried out in 2008, 2010, and 2011, providing a total of five new seismic profiles constraining the location and character of the Meeman-Shelby Fault (MSF), about 9 km west of Memphis, Tennessee, in the Central U.S. The MSF is the best documented fault closest to Memphis yet discovered and shows a recurrent fault history. The fault, as imaged by the reflection profiles, is ~45 km long, strikes N25°E, and dips west-northwest ~83°, exhibiting an up-to-the-west sense of motion with a possible right-lateral strike-slip component. The data show that on average, the MSF offsets the Paleozoic unit ~77 m and folds the top of the Cretaceous unit and the Paleocene-Eocene Wilcox Group ~44 and ~25 m, respectively. One seismic profile acquired along the Mississippi River images the bottom of the Quaternary alluvium warped up ~28 m, indicating recent activity of the MSF. Calculated vertical slip rates of the MSF during the deposition of the Upper Cretaceous, Paleocene, Eocene, and Quaternary sediments are 0.0022, 0.0010, 0.0004, and 0.2154 mm/yr, respectively, suggesting an increase in fault activity during the Quaternary. Consistent with the present stress field and the deformation of the New Madrid seismic zone fault system, we interpret the MSF as a *P* shear fault in the context of a left-stepping, right-lateral constraining strike-slip fault system under a nearly east-west oriented compressional stress field. Source scaling estimates indicate that the MSF is capable of generating a *M*6.9 earthquake if rupturing in one event.

Citation: Hao, Y., M. B. Magnani, K. McIntosh, B. Waldron, and L. Guo (2013), Quaternary deformation along the Meeman-Shelby Fault near Memphis, Tennessee, imaged by high-resolution marine and land seismic reflection profiles, *Tectonics*, *32*, 501–515, doi:10.1002/tect.20042.

1. Introduction

[2] The plate tectonic theory provides a framework to interpret earthquakes located along plate boundaries, but it fails to explain the earthquakes that occur inside the tectonic plates, such as those occurring along the New Madrid seismic zone (NMSZ), located in the central U.S. (Figure 1). Here the present, historical, and prehistorical seismicity [*Johnston and Schweig*, 1996; *Tuttle et al*., 2002; *Chen et al*., 2006] appears to conflict with the apparent low rates of deformation at the surface (less than ~1.4 mm/yr) [*Newman et al*., 1999; *Calais et al*. 2006; *Calais and Stein*, 2009; *Vidale et al*., 2011; *Frankel et al*., 2012]. A hypothesis proposed to resolve this conflict is that deformation may be focused in different areas at different times and that the present seismicity might not reflect the long-term behavior of the seismogenic faults in the area [*Pratt*, 1994; *McBride et al*., 2002; *Crone et al*., 2003; *Stein and Newman*, 2004; *Stein*, 2007; *Calais and Stein*, 2009; *Stein et al*., 2009; *Liu et al*., 2011]. One important implication of this hypothesis is that seismogenic faults might exist outside the NMSZ, buried beneath the sediments of the Mississippi Embayment (Figure 1), potentially posing a seismic hazard to the region. Evidence corroborating this hypothesis is also provided by earthquake-induced liquefaction features observed at several locations in the Mississippi Embayment (e.g., in the Wolf River floodplain in Memphis, Tennessee [*Broughton et al*., 2001], near Marianna, Arkansas [*Tuttle et al*., 2006], and near the Arkansas-Louisiana border [*Cox et al*., 2007]). The age of these venting episodes shows no correlation with the age of large earthquakes in the NMSZ (clustered at A.D. 900, A.D. 1450, and in 1811–1812 [*Tuttle et al*., 2002]) and together with their location (in some cases identified at distances up to ~350 km from the NMSZ) indicate the existence of additional seismic sources outside the NMSZ active during the Quaternary. As increasing evidence for multiple faults active at different times in the central U.S. emerges [*Howe and Thompson*, 1984; *Howe*, 1985; *Crone et al*., 1995; *Luzietti et al*., 1995; *Williams et al*., 1995;

[1]Center for Earthquake Research and Information (CERI), University of Memphis, Memphis, Tennessee, USA.
[2]Institute for Geophysics, University of Texas at Austin, Austin, Texas, USA.
[3]Department of Civil Engineering, University of Memphis, Memphis, Tennessee, USA.

Corresponding author: Y. Hao, Center for Earthquake Research and Information (CERI), University of Memphis, 3890 Central Ave., Memphis, TN 38152, USA. (yhao@memphis.edu)

0278-7407/13/10.1002/tect.20042

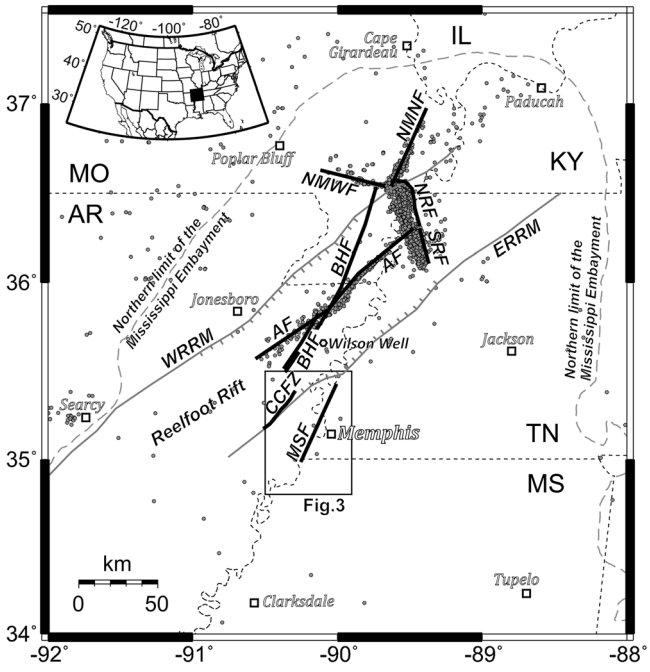

Figure 1. Regional map of the main tectonic features in the Mississippi Embayment. The location of the Western Reelfoot Rift Margin and the Eastern Reelfoot Rift Margin (WRRM and ERRM, respectively) is based on potential field data interpretations of *Hildenbrand and Hendricks* [1995]. Seismically active faults in the embayment include the New Madrid North Fault (NMNF), the New Madrid West Fault (NMWF), the Reelfoot Thrust, divided into the North Reelfoot Fault (NRF) and the South Reelfoot Fault (SRF), and the Axial Fault (AF) [*Johnston and Schweig*, 1996; *Csontos and Van Arsdale*, 2008; *Tavakoli et al*., 2010; *Pratt*, 2012]. Additional relevant faults imaged by high-resolution surveys include the Bootheel Fault (BHF), the Crittenden County Fault Zone (CCFZ), and the Meeman-Shelby Fault (MSF) [*Schweig and Marple*, 1991; *Crone et al*., 1995; *Guccione et al*., 2005; *Luzietti et al*., 1995; *Williams et al*., 1995; *Williams et al*., 2001; *Odum et al*., 2010]. Dots indicate seismicity (CERI New Madrid Earthquake Catalog 1996–2012, *M*0.2–*M*4.7).

Stephenson et al., 1995; *Schweig and Van Arsdale*, 1996; *Odum et al*., 1998; *Williams et al*., 2001; *Parrish and Van Arsdale*, 2004; *Baldwin et al*., 2005; *Bexfield et al*., 2005; *Velasco et al*., 2005; *Bexfield et al*., 2006; *Harris and Sorrells*, 2006; *Csontos et al*., 2008; *Harris*, 2009; *Odum et al*., 2010], it becomes crucial to understand the location, timing, and character of these faults, whether a pattern exists among the activity of the fault systems, and the tectonic mechanism(s) that control the localization of deformation along them.

[3] In order to test the aforementioned hypothesis and to identify the faults buried beneath the unconsolidated sediments of the Mississippi Embayment, a series of high-resolution seismic reflection surveys were carried out along and near the Mississippi River between 2008 and 2011 as part of the Mississippi River Project [*Magnani and McIntosh*, 2009]. Here we present the results of five profiles that imaged a ~45 km long fault both on land and along the river, interpreted as the Meeman-Shelby Fault (MSF), near Memphis, Tennessee. In addition to seismic multichannel reflection data, coincident sub-bottom profiler (CHIRP) data were acquired during the marine survey along the Mississippi River to help constrain the detailed shallow structure and the more recent deformation history of the imaged MSF.

2. Geologic Setting

2.1. Main Geologic Features in the Study Area

[4] Our study area is located in the Mississippi Embayment, along the southeastern margin of the failed Paleozoic Reelfoot Rift (Figures 1 and 3). The Mississippi Embayment is a ~200–400 km wide alluvial plain, representing the northern extension of the Gulf Coastal Plains reaching into the interior of the North American continent as far north as Cairo, Illinois. The embayment is filled by gently southward dipping unconsolidated Cretaceous, Tertiary, and Quaternary sediments topped by the Mississippi River alluvium [*Stearns*, 1957; *Van Arsdale*, 2009; *Hardesty et al*., 2010]. The thickness of the unconsolidated sediments in the embayment is ~1 km near Memphis [*Van Arsdale and Ellis*, 2004; *Ge*, 2009] and reaches ~2 km to the south, where the embayment merges with the Gulf Coastal Plains [*Stearns*, 1957; *Cox and Van Arsdale*, 1997, 2002; *Van Arsdale and Ellis*, 2004]. The lower boundary of the embayment section is marked by an unconformity of Cretaceous sequences on lower Paleozoic rocks.

[5] The major paleotectonic structure of the study region is the Reelfoot Rift, a 300 km long, 70 km wide northeast-striking crustal feature buried beneath the Mississippi Embayment sediments. The structure has been constrained by gravity, magnetic, and borehole data [*Thomas*, 1991; *Hildenbrand and Hendricks*, 1995], and it is commonly interpreted as a Late Precambrian-Early Cambrian failed rift associated with the breakup of the supercontinent Rodinia and the opening of the Iapetus Ocean [*Burke*, 1980; *Johnston and Kanter*, 1990; *Van Arsdale*, 2009; *Thomas*, 2010, 2011]. Studies show that the Reelfoot Rift was reactivated during the Cretaceous, when magma intruded the rift sequences [*Ervin and McGinnis*, 1975; *Hildenbrand and Hendricks*, 1995; *Van Arsdale*, 2009]. This paleotectonic structure appears to play a role in focusing the deformation in the Central U.S., as the 1811–1812 New Madrid earthquakes, with the estimated magnitude ranging from *M*7 to *M*8 [*Nuttli*, 1973; *Johnston and Schweig*, 1996; *Hough et al*., 2000], and the current seismicity in the NMSZ (Figure 1) have been attributed to the reactivation of basement faults within the Reelfoot Rift [*Braile et al*., 1986; *Johnston and Kanter*, 1990; *Parrish and Van Arsdale*, 2004; *Csontos et al*., 2008].

[6] The NMSZ, represented by the present cluster of seismicity within the Reelfoot Rift (Figure 1), is interpreted as a right-lateral strike-slip fault zone with a left-stepping restraining bend [*Russ*, 1982; *Chiu et al*., 1992; *Pratt*, 1994; *Csontos and Van Arsdale*, 2008; *Tavakoli et al*., 2010]. The north-northeast-trending dextral strike-slip Bootheel Fault [*Schweig and Marple*, 1991; *Guccione et al*., 2005] links the two northeast-trending arms of the NMSZ seismicity, and it has been interpreted as one of the 1811–1812 historic earthquakes coseismic faults within the NMSZ system, despite the lack of present seismic activity. Additional prominent features in the study area (Figure 3) are the Eastern Reelfoot Rift Margin (ERRM)

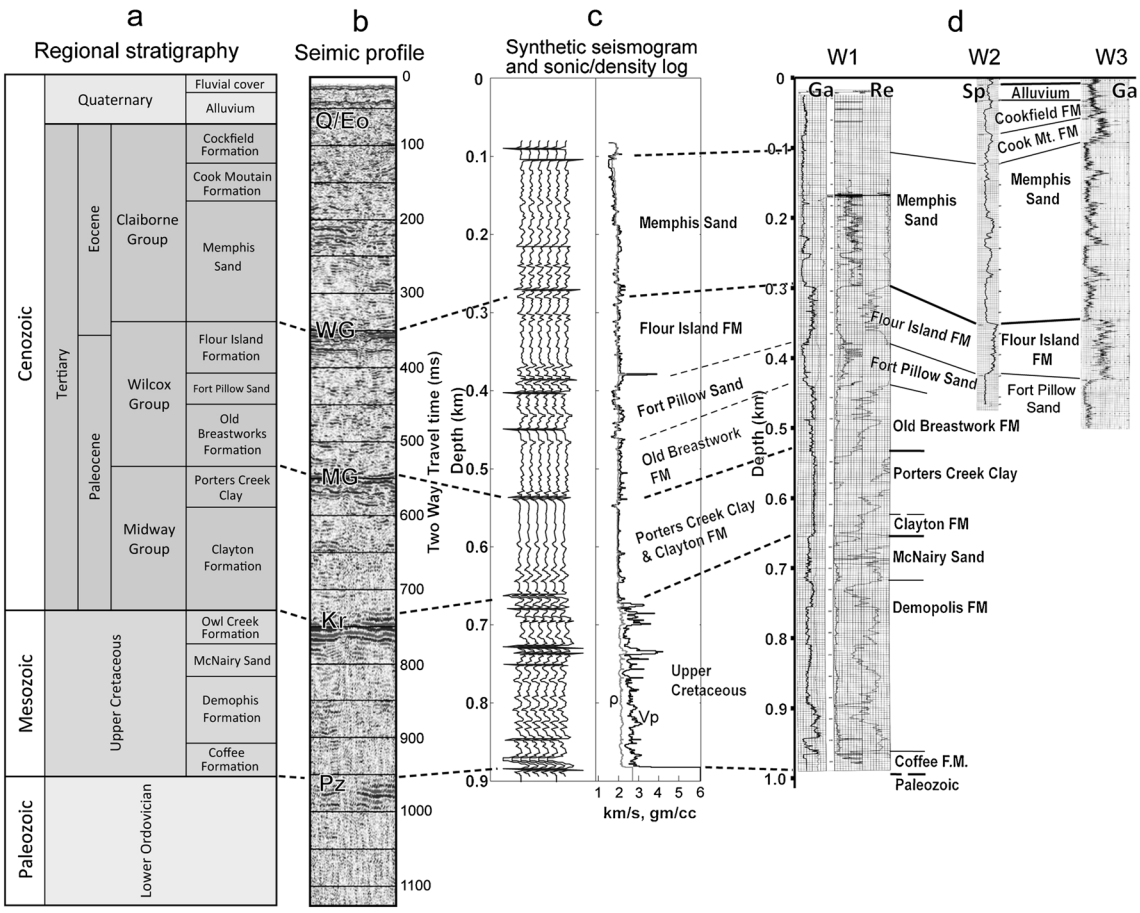

Figure 2. (a) Regional stratigraphy of the unconsolidated sediments in the Mississippi Embayment with formation names and correlation (b) with seismic data in the study area, (c) with the synthetic seismogram (left) derived from the Wilson Well 2-14 sonic log (right), and (d) with three local well logs (W1: Gamma ray and resistivity; W2: self-potential; W3: Gamma ray). The stratigraphy column was derived from studies in this region [*Saucier*, 1994; *Luzietti et al*., 1995; *Parrish and Van Arsdale*, 2004] and modified according to the interpretations of the well logs in Figure 2d. The *P* wave velocity model for time-to-depth conversion of the seismic profiles was derived from the Wilson Well 2-14 sonic log in Figure 2c [*Langston*, 2003].

and the Crittenden County Fault Zone (CCFZ) [*Luzietti et al*., 1995]. The northeast-trending ERRM consists of two major down-to-the-west normal basement faults, which show evidence of reactivation and inversion during the Tertiary as reverse faults [*Parrish and Van Arsdale*, 2004; *Cox et al*., 2006]. Located along the trend of the ERRM, the CCFZ is a northeast-striking reverse fault, with a proposed dextral strike-slip component, that was active at least during the middle to late Eocene and possibly during the Quaternary (probably Holocene) [*Luzietti et al*., 1995; *Williams et al*., 1995].

[7] Along the ERRM, northeast of the CCFZ, a high-resolution Mini-Sosie seismic reflection survey imaged the Meeman-Shelby Fault (MSF) [*Williams et al*., 2001] (Figure 1 and line L1 in Figure 3), interpreted as a steep westward dipping fault (~75°) with an up-to-the-west sense of displacement. The fault offsets the Paleozoic and the Cretaceous sections 70 and 40 m, respectively, and warps the Paleocene and the Eocene sediments 50–60 m. Unfortunately, this survey failed to image the Eocene/Quaternary unconformity and the Quaternary alluvium, leaving the Quaternary timing of the deformation of the MSF at this location unconstrained. To constrain the MSF trend, a higher-resolution 1.5 km long hammer-source *P* wave seismic survey and a 1.1 km long *S* wave seismic survey were carried out at the same site [*Odum et al*., 2010]. This survey re-imaged the MSF, and the MSF was interpreted as a N13°W striking fault representing the eastern boundary of the Joiner Ridge, a subsurface uplift located between the eastern Reelfoot Rift margin and the intra-rift axial fault zone, proposed to represent a compressional step over structure similar to the Reelfoot Fault to the north [*Csontos et al*., 2008; *Odum et al*., 2010]. Also, this survey failed to constrain recent (post-Eocene) history of deformation of the MSF.

2.2. Stratigraphy

[8] The shallow (~1.5 km deep) stratigraphy of the study area records the evolution of this portion of the North American continent from the end of the Paleozoic rifting to the modern alluvial plain and consists predominantly of sediments, deposited both in marine and continental environments.

[9] The Ordovician limestones and dolomites at the base of the stratigraphic column are separated from the overlying Upper Cretaceous marls and sandy limestones by a regional unconformity (Figure 2), recording extensive denudation

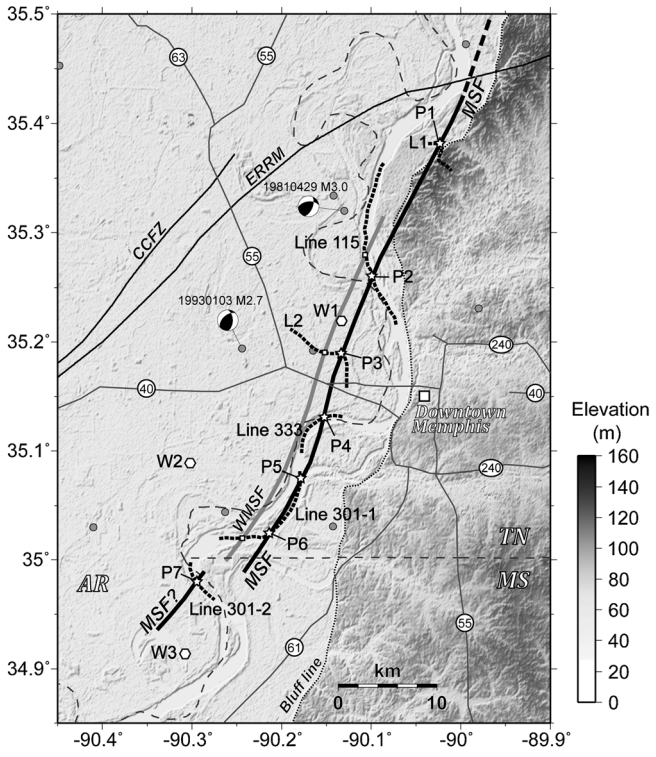

Figure 3. Topography map of the study area showing the extent of the MSF (heavy black line) as imaged by the five new seismic profiles and the existing seismic data (L1). CCFZ: Crittenden County Fault Zone; ERRM: East Reelfoot Rift Margin [*Hildenbrand and Hendricks*, 1995]. Heavy dashed lines indicate land and marine multichannel seismic reflection lines. Dots show seismicity in the area (CERI New Madrid Earthquake Catalog 1974–2012, *M*1.3–*M*3.0). Focal mechanism solutions by *Chiu et al*. [1997]: event 19810429 (strike N83°E, dip N51°W, rake 137°, right-lateral strike-slip fault with thrust component, 6.3 km depth, *M*3.0); event 19930103 (strike N49°E, dip N51°W, rake 126°, right-lateral strike-slip fault with thrust component, 17.3 km depth, *M*2.7). Hollow hexagons represent boreholes (W1–3). Stars show surface projections (P1–7) of the MSF. Squares represent surface projections of the secondary eastward-dipping fault (thick gray line), the West Meeman-Shelby Fault (WMSF). The thin gray lines with numbered labels are the interstate and U.S. routes.

that removed all the late Paleozoic and early Mesozoic strata [*Van Arsdale*, 2009; *Thomas*, 2010]. Another unconformity separates the Upper Cretaceous section from the Tertiary units, consisting of the Paleocene Midway Group (clays), the Paleocene-Eocene Wilcox Group (sands and clays), and the Eocene Claiborne Group (sands, silts, and clays) [*Saucier*, 1994; *Parrish and Van Arsdale*, 2004; *Velasco et al*., 2005; *Van Arsdale*, 2009]. Additional secondary unconformities within the Tertiary units record the Paleocene regression and the Eocene marine transgression from the south. At the top of the stratigraphic sequence, the Quaternary sediments lie unconformably over the Eocene Claiborne Group.

[10] The stratigraphy of Quaternary sediments changes from the uplands, east of the bluff line, to the alluvial plain, west of the bluff line (Figure 3). East of the bluff line, the Quaternary units contain the Pliocene-Pleistocene Upland Complex (sands and gravels) and the Late Pleistocene loess (silts). The Upland Complex (also called Lafayette gravel) is a sand and gravel alluvial terrace of the ancestral Mississippi River that is erosionally inset into the underlying Tertiary units [*Fisk*, 1944; *Saucier*, 1994; *Van Arsdale et al*., 2007]. West of the bluff line in the alluvial plain, the Quaternary stratigraphy mainly consists of Pleistocene river terraces and Holocene meander belt deposits (clays, silts, and sands) [*Autin et al*., 1991; *Saucier*, 1994; *Parrish and Van Arsdale*, 2004; *Velasco et al*., 2005; *Rittenour et al*., 2007]. Although the basal alluvium has not been dated, it has been suggested, based on the Late Pleistocene river valley evolution and on wells in proximity of the Mississippi River channel [*Fisk*, 1944; *Autin et al*., 1991; *Saucier*, 1994; *Blum et al*., 2000; *Van Arsdale*, 2000; *Calais et al*., 2010], that the base of the Quaternary section near Memphis is probably no older than Late Pleistocene or perhaps even as young as Holocene. The Quaternary alluvium, which consists of a basal sand and gravel floodplain and upper sand, silt, and clay floodplain facies [*Fisk*, 1944; *Saucier*, 1994; *Rittenour et al*., 2007], directly overlies on the Eocene upper Claiborne Group in the area of the survey lines (Figure 3).

[11] The stratigraphy used for the interpretation of the seismic profiles (Figure 2) was derived from regional stratigraphic studies [*Fisk*, 1944; *Saucier*, 1994; *Luzietti et al*., 1995; *Parrish and Van Arsdale*, 2004], as well as interpretations of three well logs of self-potential, resistivity, and Gamma ray located in proximity of the seismic lines. Time-to-depth conversion of seismic profiles was performed using a *P* wave velocity model derived from the Wilson 2-14 Well sonic log (Figure 1) [*Langston*, 2003].

3. Seismic Data Acquisition and Processing

3.1. Marine Seismic Surveys

[12] The marine seismic reflection data presented here were acquired as part of the Mississippi River Project during two field campaigns, in the summer of 2008 and 2011. The 2008 campaign acquired multichannel seismic reflection data, while the 2011 campaign acquired coincident multichannel and CHIRP reflection data. Below we describe the acquisition and processing of these data sets.

3.1.1. Multichannel Reflection Data

[13] The 2008 and 2011 high-resolution marine seismic surveys were carried out along the Mississippi River to take advantage of marine seismic acquisition (time-efficient, low cost compared to land acquisition) to image a large portion of the Mississippi Embayment, while avoiding the pitfalls of land acquisition (e.g., source generated noise such as "ground roll") and statics problems. However, acquiring seismic reflection data along the Mississippi River is a challenging task due to the strong and changing current, the heavy ship traffic, and the presence of in-channel man-made barriers and structures (dikes), and bank erosion control features (revetments) along the narrow navigable channel. Only one survey [*Shedlock and Harding*, 1982] attempted a regional profile along the Mississippi River in 1981 and achieved consistent penetration of 0.8–1.0 s two-way travel time (TWT), imaging with fairly good continuity the top of the Paleozoic and the Cretaceous sections and intermittently the Tertiary sediments. The 1981 survey had mixed results with imaging the shallow Cenozoic units, precluding any attempt to document recent faulting

Table 1. Acquisition Parameters of the Seismic Surveys

Parameters	Mississippi River Project	1981 USGS[a] River Survey	2010 Land Survey
Source	Airgun, Sercel Mini GI/15/15 in^3, 13.79 MPa	Airgun, Bolt 40 in^3	9990 kg Mini Vibe, 20–220 Hz, 12 s, upsweep
Shot interval	2–6.5 m, 9 m[b]	5–10 m	10 m
Receiver	Streamer: 75 m long, 24 channels	Streamer: 120 m long, 12 channels	Geophone: 40 Hz, vertical, 720 m long, 144 channels
Receiver interval	3.125 m	10 m	5 m
First receiver offset	3–6 m	61 m	10 m
Sampling interval	0.5 ms	0.5 ms	1 ms
Samples per trace	3000, 4000	2000	2000 (correlated)
Stacking fold	6–16, 8	6–12	36
CDP[a] interval	1.6 m, 3.125 m	5–10 m	2.5 m
Survey line length	300 km, 420 km	240 km	10 km

[a]USGS, U.S. Geological Survey; CDP, common depth point.
[b]Left (2–6.5 m) and right (9 m) values refer to the 2008 and 2011 campaigns, respectively; same as the rest of the data.

associated with ongoing deformation. To meet the goal of the Mississippi River Project (i.e., understanding the long-term distribution of Quaternary deformation in the Mississippi Embayment), the 2008 and 2011 surveys were acquired with a different geometry than the *Shedlock and Harding* [1982] survey and used a more advanced seismic source (Table 1). The geometry of the river acquisition was designed to achieve high-resolution imaging of the sedimentary layers from the bottom of the river down to a depth of up to ~2 km. The 3–6 m minimum source-receiver offset ensured detection of reflections of shallow structures, and the higher number of hydrophones resulted in a denser spatial sampling. The high quality of the 2008 and 2011 data is also the result of a novel procedure to reduce the environmental noise during acquisition along the river. To reduce the speed through the water of the seismic equipment (and therefore the noise resulting from it), the acquisition was carried out by slowly drifting backward downriver, while facing upriver, rather than moving against the river current as was done in the previous survey [*Magnani and McIntosh*, 2009]. The 2011 survey partially overlaps with the 2008 survey, to provide CHIRP coverage to the section of the river previously imaged only by multichannel data.

[14] The seismic reflection data were processed using a flow resulting from careful analysis and testing (Table 2). In addition to the objective of improving the general S/N ratio of the data, specific goals of the processing steps were as follows: (1) removal/attenuation of coherent noise generated by artifacts along the river bottom and banks, (2) attenuation of water bottom multiple reflections, and (3) enhancement of the coherency of reflectors. After preprocessing and assigning the geometry, an amplitude spike editing procedure was applied to attenuate the high-amplitude/high-frequency pulses of noise (spikes) generated by artifacts located at the river bottom and along the banks (e.g., the flow control dikes and revetments). A time-variant band-pass filter was applied to eliminate high-frequency noise in the deeper portion of the section and to preserve the signal in the shallow record. A water bottom multiple reflection attenuation process was tested during the data analysis and not applied to the presented profiles. The process successfully attenuates the river bottom multiples at depth, but it is less effective in preserving the reflectors at shallow depth (e.g., the base of the Quaternary unit), which are among the main target of our investigation. After normal moveout correction and stacking, a FX deconvolution was applied to enhance the coherency of the reflectors. No substantial improvement in S/N was observed after F/K

Table 2. Processing Flow of the Mississippi River Project Seismic Data[a]

Process	Parameters and Descriptions
Data reformat	Convert from SEGY to FOCUS internal
Geometry	Sources, receivers, and CDPs definition
Band-pass filter	30–60–400–600 Hz (Ormsby minimum phase)
Amplitude recovery	Correction for spherical divergence and transmission losses
Mute	Top mute (first arrivals and refracted phases removal)
Amplitude spike editing	River dikes and the revetment noise attenuation
Time-variant filter	1–150 ms, 30–60–400–600 Hz; 400–1500 ms, 25–40–250–350 Hz (Ormsby minimum phase)
CDP sort	Sort to CDP domain
Velocity analysis	Build a 2-D stacking velocity model for NMO correction
NMO correction	Correction applied using the RMS velocity model
CDP stack	Eightfold nominal
FX deconvolution	Enhance coherence of reflectors
Time-to-depth conversion	Velocity model used: 2-D *P* wave velocity model derived from the Wilson 2-14 Well sonic log

[a]NMO, normal moveout; FX, frequency-offset.

Table 3. Processing Flow of the 2010 Land Seismic Data[a]

Process	Parameters and Descriptions
Data reformat	Convert from SEGY to ProMAX internal
Vibroseis correlation	Total correlated trace length: 2000 ms
Trace editing	Remove noisy traces and correct reversed traces
Data combination	Stack two shot gathers into one
Geometry	Crooked line geometry with 2.5 m bin size
Band-pass filter	10–24–150–177 Hz (Ormsby minimum phase), 60 Hz Notch
Top mute	Remove first arrivals and refractions
Internal mute	Remove data within surface wave cone
Air blast attenuation	348 m/s air wave velocity
CDP sort	Sort to CDP domain
Velocity analysis	Build a velocity model for NMO correction, 3 CDPs for super gather formation
NMO correction	100% stretch mute
Band-pass filter	Same as the one above
AGC	Equalize the trace amplitudes, 150 ms
Eigenvector filter	0–60% eigenimage accepted
CDP stack	36 fold nominal
Time-variant filter	0–70 ms: 45–55–150–177 Hz; 150–550 ms: 30–45–150–170 Hz; 700–2000 ms: 10–24–140–160 Hz (Ormsby minimum phase)
Time-to-depth conversion	Conversion using the 2-D *P* wave velocity model derived from the Wilson 2-14 well sonic log

[a]AGC, automatic gain control.

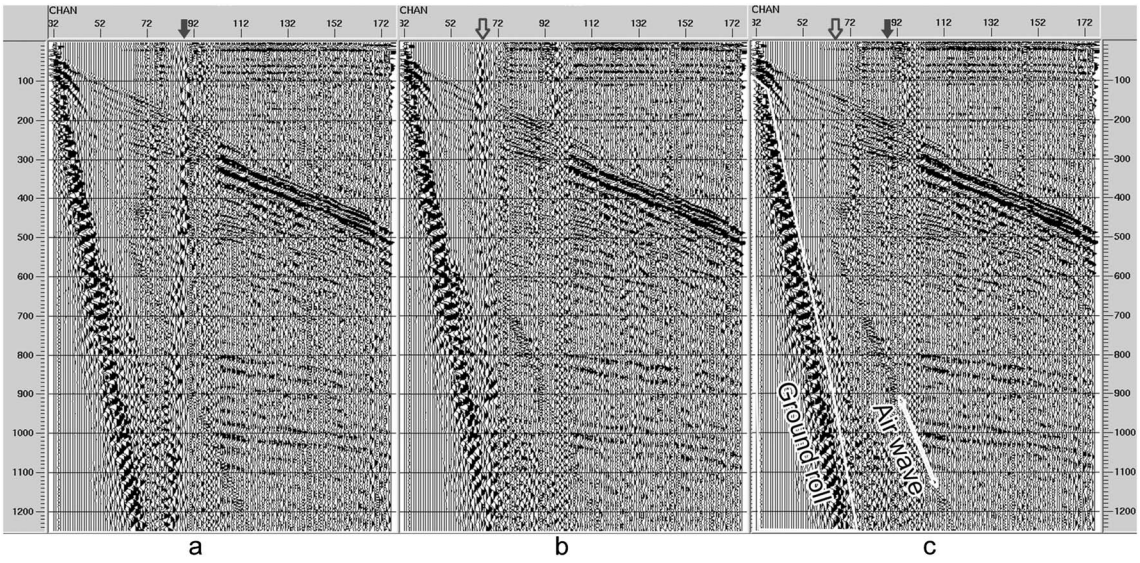

Figure 4. Shot gather samples acquired as part of the 2010 land survey showing the correlation/stack process at a single shot point. (a) First shot gather after Vibroseis correlation and band-pass filter (10–24–150–177 Hz); (b) second shot gather acquired at the same shot point and with identical processing; (c) stacking result of the two shot gathers. Traffic noise (marked by the solid and hollow arrows) has been effectively attenuated after stacking. Reflectors are visible from 200–1100 ms. Clear reflectors between 800–900 and 1000–1100 ms are interpreted as the top of the Upper Cretaceous sediments and the top of the Paleozoic rocks, respectively. Ground-roll noise is visible as a high-amplitude, low-frequency energy at near offset. The air wave energy is visible as the high-frequency, low velocity (335 m/s) linear arrival.

migration with a constant velocity field of 1500 m/s; therefore, only stacked profiles are shown here.

[15] The dominant frequency of the marine data ranges between 100 and 300 Hz, which results in vertical resolutions of ~2–5 m in the Tertiary and Cretaceous sediments and ~15 m in the Paleozoic rocks. Horizontal resolution ranges between ~25 and 70 m in the Tertiary and Cretaceous sediments and ~160 m at the top of the Paleozoic rocks.

[16] To more accurately constrain the deformation history of the MSF, data were depth converted after stacking using a *P* wave velocity field derived from the Wilson Well sonic log (Figure 2c). The 2-D velocity field was derived by projecting the time-converted Wilson Well 1-D velocity function on the seismic profiles and calibrating the key regional seismic markers/reflectors (Figures 2b and 2c).

3.1.2. CHIRP Data

[17] The CHIRP data were collected coincident with the multichannel reflection data along the Mississippi River using an Edgetech SB-512i echo sounder floating at a depth of ~1.5 m in the water and using a source with a frequency of 0.7–1.2 kHz to image the ultra-shallow structures (within the first 50 m) beneath the river. A transducer was used to record the towing depth of the CHIRP to remove the effects of towing depth variations on the imaged structures.

3.2. Land Seismic Survey

[18] The Mississippi River Project imaged the MSF at five river crossings. To constrain the extension of the MSF on land and verify the northeast trend of the fault suggested by the marine data, a high-resolution seismic reflection survey was carried out in the summer of 2010 near West Memphis, Arkansas, between two river crossings where the fault was imaged. The acquisition parameters for the land survey were designed to be similar to those used for the Mississippi River Project (Table 1) to facilitate the comparison between the two data sets. The profile was acquired using a Vibroseis seismic source by the NEES consortium at the University of Texas at Austin, and a Geode recording system by the U.S. Geological Survey (USGS) Near Surface Imaging Group in Golden, CO. A minimum of two shots were recorded at each shot station to increase the S/N ratio and reduce random noise. High water tables and compact near-surface clays and sands in

Table 4. Estimates of Deformation and Slip Rate of the MSF

	Cumulative Deformation (m)					Vertical Deformation (m)							
Section	155	L2	333	301-1	Mean	155	L2	333	301-1	Mean	Average Net Slip (m)	Time Span (Myr)	Vertical Slip Rate (mm/yr)
Quaternary	-	-	-	-	-	28	-	-	-	28.0	38.0	0.13	0.2154
Eocene	28	-	-	-	28	19	21	19	12	17.8	24.1	45	0.0004
Paleocene	47	21	19	12	25	14	21	26	17	19.5	26.5	20	0.0010
Cretaceous	61	42	45	29	44	66	14	26	23	32.3	43.8	15	0.0022
Paleozoic	127	56	71	52	77	-	-	-	-	-	-	-	-

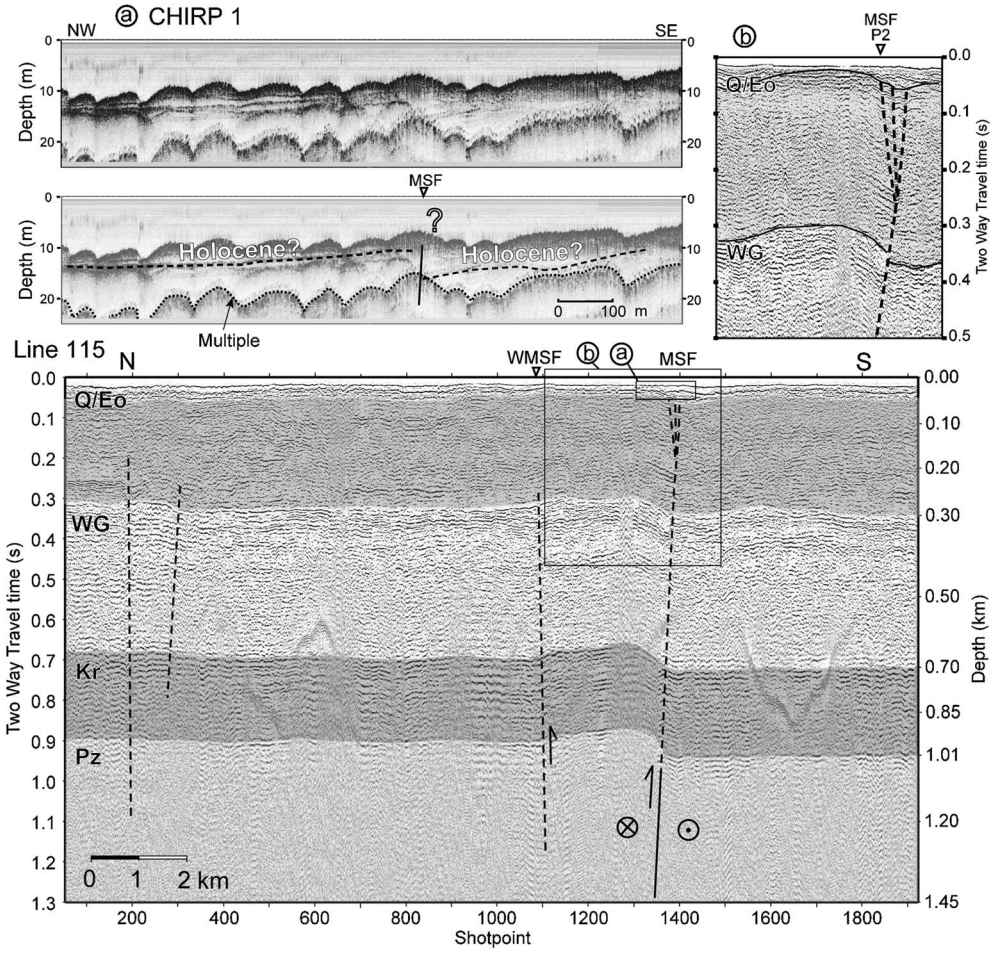

Figure 5. Multichannel seismic reflection Line 115 and CHIRP profile CHIRP 1. Black solid and dashed lines indicate interpreted faults. Line 115 is a two-way travel time (TWT) profile with estimated values of depth based on time-to-depth conversion. Pz: Paleozoic; Kr: Cretaceous; WG: Paleocene-Eocene Wilcox Group; Q/Eo: Quaternary-Eocene unconformity. P2 and the triangle indicate the surface location of the MSF, the same as the WMSF (see Figure 3 for location). (a) CHIRP profile showing a reflector possibly offset by ~6 m above the surface projection of the MSF. (b) Close-up of Line 115 showing the details of the deformed WG and the Q/Eo boundary.

this region provided good conditions for energy penetration in the unconsolidated sediments [*Luzietti et al*., 1995].

[19] The seismic data were processed using a tested processing flow (Table 3) for high-resolution land seismic reflection data in the unconsolidated sediments of the Mississippi Embayment. After Vibroseis correlation, which resulted in 2 s long fully correlated traces, noisy traces were edited out of the data set, and two clean shot gathers at each shot station were stacked to enhance the S/N ratio. This step proved especially effective in suppressing the random ambient noise, such as the incoming traffic along the nearby road (Figure 4). Following the common depth point (CDP) sorting, normal moveout (NMO) correction, and stacking, data were depth converted to obtain the depth information for critical reflectors similarly to the marine data.

[20] The dominant frequency of the land seismic data ranges from 40 to 50 Hz after data processing. The vertical resolution in the Tertiary and Cretaceous sections is ~10–15 m and ~35 m at the top of the Paleozoic section. The horizontal resolution ranges between ~50–140 m in the Tertiary and Cretaceous sediments and ~250 m in the Paleozoic rocks.

4. Interpretation

[21] The Mississippi River Project and the 2010 land survey provide five new profiles of unprecedented high quality that constrain the location, character, and extent of the MSF (Figure 3). These profiles, in addition to the seismic profiles by *Williams et al*. [2001] and *Odum et al*. [2010], image the MSF for ~45 km. Here we present the TWT version of the seismic profiles to facilitate the interpretation of the details of the low velocity portions of the unconsolidated sediments. Vertical slip rates (Table 4) for the MSF were calculated from displacements estimated from the depth converted profiles.

4.1. Line 115

[22] The 16 km long north-south trending Line 115 (Figures 3 and 5) was acquired during the 2008 campaign. Clear continuous reflectors are visible throughout the profile from the top of the Paleozoic rocks (Pz, at ~1 km depth), the top of the Upper Cretaceous sediments (Kr, at ~0.7 km depth), to the top of the Paleocene-Eocene Wilcox Group (WG, at ~0.3 km depth). Also, the reflector marking the unconformity between

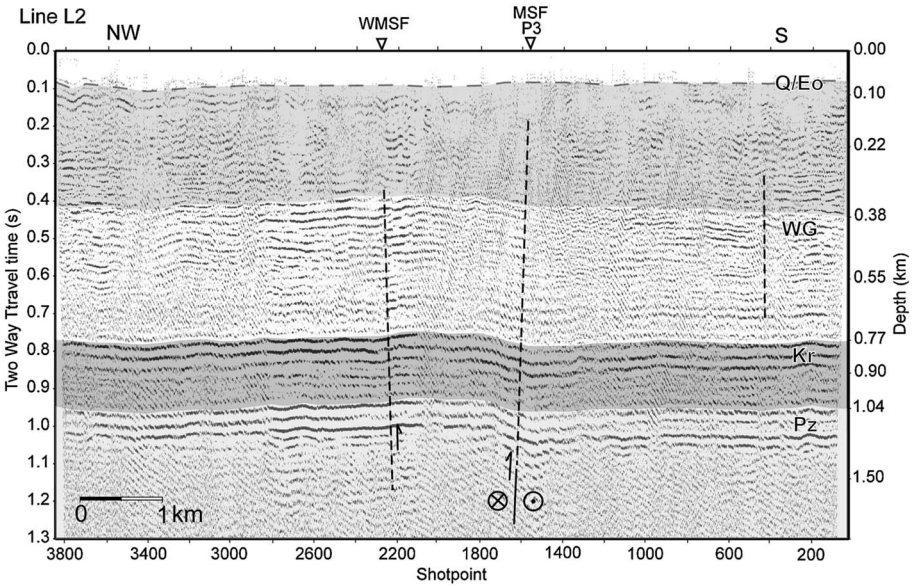

Figure 6. Land seismic profile Line L2 and interpretation (see Figure 3 for location). Labels of stratigraphy are the same as Line 115 in Figure 5. Triangles and labels show the surface projections of the MSF and the WMSF. The Q/Eo boundary is estimated according to local stratigraphy.

the Quaternary alluvium and the Eocene deposits (Q/Eo) is intermittently traceable throughout the seismic line. Along the profile between shot points 1300–1400, a zone of deformation, interpreted as the MSF, crosses the entire sedimentary section, from the Paleozoic unit to the Quaternary alluvium. The MSF is interpreted as a fold in the unconsolidated sediments associated with a fault at depth. The fault and the zone of deformation have an apparent dip of 79° to the northwest on the seismic profile and display an up-to-the-west sense of motion. A true dip of 83° is calculated from the apparent dip and the intersection angle between the seismic line and the fault strike. The seismic data show the Paleozoic and the Cretaceous units folded ~127 and ~61 m in relief, respectively. The top of the WG is also warped ~47 m. The shallow units at the MSF (Figure 5b) appear to have been deformed consistently with the older units, as the base of the Quaternary alluvium is folded ~28 m on the profile. The deformation at the base of the Quaternary alluvium is significant evidence for recent activity of the MSF. The consistent decrease of deformation from the top of the Paleozoic rocks to the Quaternary alluvium suggests prolonged history of deformation of the MSF throughout the Cretaceous, Tertiary, and Quaternary. Younger deformation (within the Quaternary) is unresolved by the multichannel seismic data.

[23] About 2.5 km north-northwest of the MSF on profile 115 (shot points 1000–1100), a second fold clearly deforms the Paleozoic rocks, the Cretaceous sediments, and the WG. Similar to the MSF, this fold is associated at depth with a south-eastward dipping fault (hereinafter the West Meeman-Shelby Fault, WMSF) showing an up-to-the-east sense of motion, which, together with the MSF to the south, defines an anticline ~2.5 km wide at the top of the Cretaceous sediments.

[24] A 1 km long CHIRP profile (Figure 5a) acquired along the surface projection of the MSF shows distinct reflectors within the Quaternary alluvium. The reflectors likely represent very recent (<500 year old) erosional or flood surfaces [*Meyer et al.*, 2011] and are visible throughout the alluvium along the Mississippi river. Along the profile, the reflector appears to be offset ~6 m above the surface projection of the MSF with the same sense of displacement as the underlying strata, although the continuity of the reflector cannot be confirmed with the available data.

4.2. Line L2

[25] Line L2 (Figures 3 and 6) was acquired during a land seismic survey conducted in 2010, near West Memphis, to identify the location of the MSF on land between the Line 115 and Line 333 river crossings and to verify the strike and continuity of the fault. The 10 km long profile successfully imaged the MSF at the predicted location (near shot point 1600), showing reflectors of the top of the Paleozoic section and the top of the Upper Cretaceous sediments folded ~56 and ~42 m at depths of ~10.4 and ~0.8 km, respectively. The top of the overlying Paleocene WG appears warped up ~21 m at the same location. Similar to the fold along Line 115, the fold visible in the unconsolidated sediments is interpreted to have developed in response to the movement along the MSF at depth, in the Paleozoic rocks. At this location, the MSF dips apparently ~80° to the west and shows an up-to-the-west sense of motion. A true dip of ~81° is calculated from the apparent dip and the intersection angle of 70°. Also, the consistent increase of offset with depth/age suggests prolonged activity throughout the Cenozoic and possibly the Late Cretaceous, which is also observed at all other locations. Similarly to Line 115, a fold with an up-to-the-east sense of motion associated with a fault at depth (WMSF) is imaged along this profile ~1.7 km west of the MSF (shot points 2200–2400).

4.3. Line 333

[26] The 7 km long Line 333 (Figures 3 and 7), acquired during the 2011 campaign and located west of Memphis, images unconsolidated sediments from the top of the Paleozoic rocks to the Tertiary units, consistently deformed along a fold

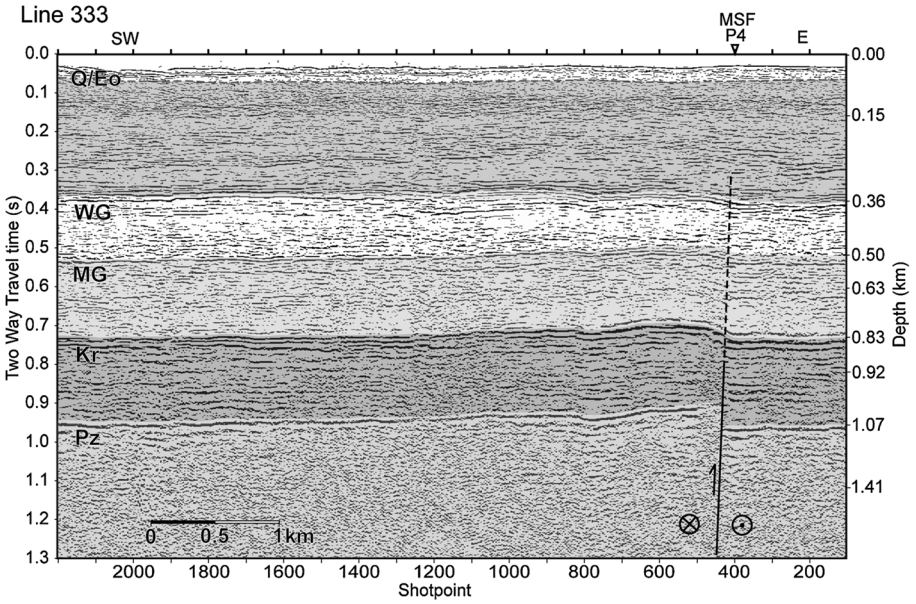

Figure 7. Seismic profile Line 333 and interpretation (see Figure 3 for location). Labels of stratigraphy are the same as Line 115 in Figure 5, with the addition of MG: Paleocene Midway Group. Triangles and labels show the surface projections of the MSF and the WMSF.

and a fault at depth interpreted as the MSF. The top of the Paleozoic rocks appears to be offset ~71 m near shot point 430, and the top of the Upper Cretaceous sediments are folded ~45 m. The reflectors marking the tops of the Paleocene Midway Group (MG) and the WG are also clearly traceable through the profile at depths of ~0.50 and ~0.36 km, and they are both warped ~34 and ~19 m, respectively, consistent with the older units. Deformation in each section decreases from the Paleozoic to the Quaternary units, suggesting consistent fault activity throughout the Cenozoic. The fault shows an up-to-the-west sense of displacement with an apparent dip of 81°, which translates to a true dip of 83° given an intersection angle of 51°.

4.4. Line 301-1

[27] Line 301-1 (Figures 3 and 8) extends northeast-southwest for ~12 km. The profile shows prominent reflectors at the top of the Paleozoic and at the top of the Upper Cretaceous sediments, as well as reflected energy from the top of the WG unit. Due to the geometry of the meander in this area, the river crosses the MSF at low angle (<15°) at two locations. Near shot point

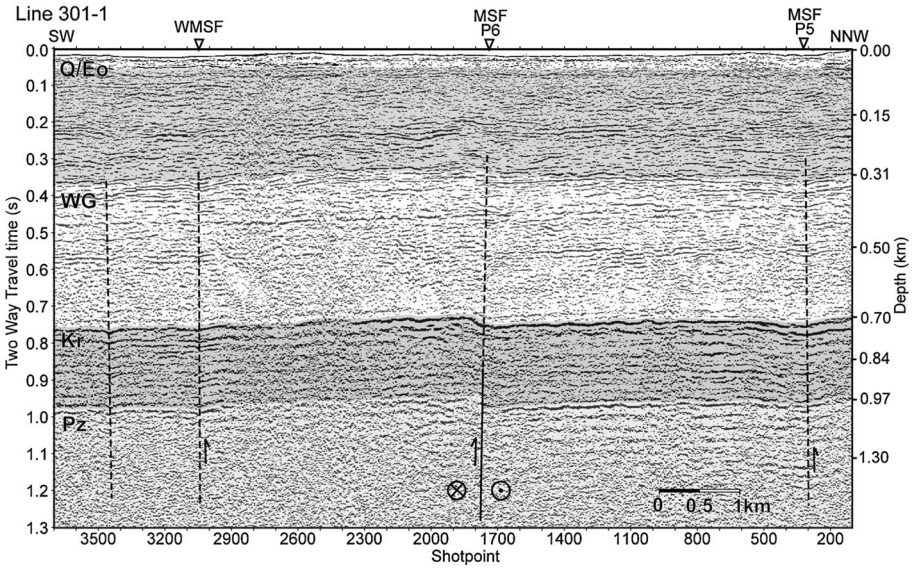

Figure 8. Seismic profile Line 301-1 and interpretation (see Figure 3 for location). Labels of stratigraphy are the same as Line 115 in Figure 5. The MSF was imaged twice on this profile since the survey line bends along the river and crosses the fault twice. Surface projections of the MSF are marked by triangles labeled with P5 and P6.

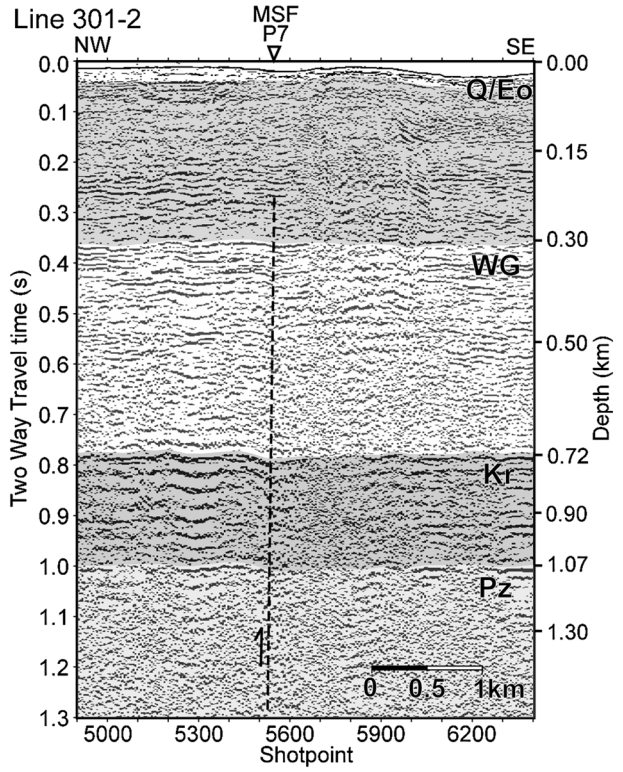

Figure 9. Seismic profile Line 301-2 and interpretation (see Figure 3 for location). Labels of stratigraphy are the same as Line 301-1 in Figure 8. Triangle and label show the surface projection of the MSF.

300, the Paleozoic, Cretaceous, and WG units appear to be gently disturbed. Because the disturbance is colinear with the MSF on the adjacent lines, we attribute this deformation to the MSF.

[28] At the center of Line 301-1 (shot points 1700–1800), the top of the Paleozoic unit is faulted ~52 m, and the Cretaceous and the WG sections are folded ~29 and ~12 m, respectively, along a fault that shows an up-to-the-west sense of displacement, consistent with the characteristics of the MSF observed on all other profiles. The apparent NNW dip of the MSF is 80° and the true dip 86°, calculated from an intersection angle of 24°. The MG reflector is intermittently traceable throughout the profile at a depth of ~0.50 km. Similarly to the other lines, an additional fault (WMSF) is traceable ~4 km west of the MSF between shot points 3000–3100. Also, the WMSF shows characteristics similar to the secondary fault observed along all the profiles, with an up-to-the-east sense of displacement and an eastward dip.

4.5. Line 301-2

[29] Line 301-2 (Figures 3 and 9) extends northwest-southeast for ~4 km. The top of the Paleozoic and Cretaceous reflectors are traceable on the profile at depths of ~1.07 and ~0.72 km, respectively, and the top of the WG reflector is intermittently traceable at ~0.3 km. The fold imaged between shot points 5500 and 5600 has an up-to-the-west sense of displacement, disturbing the top of Paleozoic, Cretaceous, and WG units, consistent with the interpreted structure of the MSF imaged to the north. This fold, however, is located to the west of the southward projection of the trace of the MSF as defined by the other profiles, suggesting that the MSF might step to the west along its southern extension, explaining the abrupt disappearance of the fault to the south along its linear trend, or the presence of a different fault.

5. Discussion

5.1. The Meeman-Shelby Fault

[30] Based on the interpretation of the seismic profiles, we conclude that the westward dipping fault identified in all the profiles is the southwestern continuation of the MSF, originally imaged by *Williams et al*. [2001] to the northeast along Line L1 (Figure 3). The locations where the fault has been identified align along a linear trend for ~45 km, striking N25°E rather than N13°W as proposed by *Odum et al*. [2010]. No substantial deformation is observed along the river at the projected crossing of the N13°W fault. The closest surface projection of the MSF to the city of Memphis is near Mound City, Arkansas, about 9 km from downtown Memphis.

[31] On each seismic profile, the fault shows a consistent up-to-the-west sense of displacement, a constant west-northwestward average dip of ~83°, and a substantial amount of deformation on each geologic unit. Along Line 115, the fault clearly deforms the base of the Quaternary alluvium of the Mississippi River, suggesting recent activity. On all the seismic profiles, a secondary fault (WMSF) has been observed west of the MSF. This fault trends parallel to the MSF and shows an up-to-the-east sense of displacement and an eastward dip. We interpret the WMSF and the MSF as part of a compressional strike-slip structure (positive flower structure) merging at depth.

[32] Because only vertical displacement can be measured on the 2-D seismic profiles, the true sense of motion cannot be calculated from the seismic reflection data alone. However, characterizing the sense and amount of motion of the fault is important to understand its tectonic significance, and it is critical for seismic hazard assessments, especially in light of evidence of the recent activity of the fault.

[33] The MSF lies south of the NMSZ and does not display appreciable seismic activity. However, some seismic events have been recorded nearby, and *Chiu et al*. [1997] reported two focal mechanism solutions in the vicinity of the fault (Figure 3), which show a reverse sense of faulting with a right-lateral strike-slip component along a northwest-dipping northeast-striking fault plane. The two events are located 6 and 10 km to the west of the MSF, with horizontal location error of 0.3–0.8 km [*Chiu et al*., 1997], and provide an estimate of the stress field orientation in this area and an interpretation of active fault mechanisms of the MSF owing to their close proximity. Consistent with the transpressional focal mechanism of nearby earthquakes and based on the evidence from seismic reflection data, we therefore interpret the MSF as a northeast-striking reverse fault with a right-lateral strike-slip component of motion, which is also consistent with the present regional N80°E compressional stress field [*Zoback and Zoback*, 1980; *Grana and Richardson*, 1996]. A right-lateral strike-slip component in addition to the predominantly reverse sense of motion has also been proposed for the adjacent CCFZ [*Luzietti et al*., 1995], located 20 km west of the MSF (Figure 3).

[34] The amount of displacement on the MSF decreases from north to south. The southern continuation of the MSF is projected to cross the Mississippi River south of the city of Memphis, Tennessee. However, no distinctive deformation has been identified on the profile along this segment of the river

(Figure 3), suggesting that the MSF might either end south of Memphis (near P6 on Figure 3) or that the fault might step to the west and correlate with the fault along Line 301-2 at P7. Because the amount of deformation at the MSF increases from south to the north, we propose that the MSF might extend further north-northeast along the river bluff east of the Mississippi River.

5.2. Deformation History of the MSF

[35] The observed increase in amount of deformation with age along the MSF from the recent alluvium to the top of the Paleozoic unit observed in the seismic profiles is consistent with a prolonged activity of the fault that spans from the Quaternary to the Late Cretaceous. To estimate the uplift rate (Table 4) of the MSF through time, the vertical displacement of the fault was measured at the top of the Paleozoic (Ordovician limestones), the Upper Cretaceous, the Paleocene (Flour Island Formation), the Eocene (upper Claiborne Group), and the Quaternary units. Because the MSF might have a significant strike-slip component in addition to the reverse motion in the present stress field, as suggested by the two nearby focal mechanism solutions [*Chiu et al*., 1997] (Figure 3), we also estimate the net slip (Table 4) for the stratigraphic markers calculated from the vertical slip (net slip = vertical slip/sin (dip)/sin(180°-rake)) using an 83° dip for the MSF derived from the interpreted seismic profiles and a rake of 132° derived from the focal mechanism solutions of *Chiu et al*. [1997]. However, due to the uncertainty of net slip estimates so calculated, here we present only the uplift rates derived from the average vertical slip for each stratigraphic section over the corresponding time period, consistently with the method and time intervals employed by *Van Arsdale* [2000], with the exception of the age of the base of the Quaternary alluvium. A conservative estimate of ~130,000 year B.P. for the age of the base of the Quaternary alluvium in the profiles is based on the Late Pleistocene Mississippi valley river evolution [*Saucier*, 1994; *Blum et al*., 2000; *Rittenour et al*., 2007]. Analysis of fluvial landforms in the Mississippi valley shows that in the Eastern Lowlands, the Pleistocene sediments might have been removed by the meltwater of the last deglaciation [*Blum et al*., 2000; *Van Arsdale et al*., 2007]. However, to be conservative, we estimate the alluvium to be Late Pleistocene (~130,000 year B.P.), although locally, it might be Holocene in age. Under this assumption, vertical slip rates of the MSF estimated for the Late Cretaceous, the Paleocene, the Eocene, and the Quaternary are 0.0022, 0.0010, 0.0004, and 0.2154 mm/yr, respectively (Table 4), suggesting an increase in fault activity during the Quaternary. Recent activity of the MSF is supported by radiocarbon ages at trench sites in Meeman-Shelby State Park, where *Cox et al*. [2013] have documented faulting, and further to the north, where *Cox et al*. [2006] identified Late Wisconsin/Holocene (<2790–2740 year B.P.) faulting at Porters Gap, Tennessee. To the south, earthquake-induced sand blows dating back to 5500 year B.P. and 6800 year B.P. are observed near the town of Marianna, Arkansas [*Tuttle et al*., 2006], 45 km along the southwest projection of the MSF. However, the distance between the currently imaged locations of the MSF and the liquefaction sites (45 km) does not favor an interpretation of the MSF as a possible seismic source for these sand blows (Tuttle, personal communication). In general, the lack of age constraint for the Quaternary section is a major source of uncertainty about the Quaternary activity of the MSF and warrants further research.

[36] Empirical relationships among the magnitude, rupture length, and displacement [*Wells and Coppersmith*, 1994] suggest that the 45 km long MSF identified in this study is capable of generating a *M*6.9 earthquake if ruptured in one event, a magnitude comparable to those suggested for the NMSZ earthquakes, and that such an event can cause an average displacement of ~0.9 m. Assuming a steady slip rate, the 38 m net slip (Table 4) in the Quaternary alluvium during the last 130,000 years translates to an average recurrence interval of ~3079 years. However, this is a maximum recurrence interval, because the magnitude of the strike slip is unconstrained and the Quaternary alluvium may be younger than 130,000 years old.

[37] The imaged length, the seismic potential, and the recent activity of the MSF as observed along the seismic profiles make the MSF one of the possible candidates for sources responsible for the earthquake-induced liquefaction features south of the NMSZ, such as the sand dikes identified in the Wolf River floodplain in Memphis, Tennessee [*Broughton et al*., 2001].

5.3. Tectonic Interpretation

[38] The close spatial relationship between the active faults of the NMSZ and the Reelfoot Rift has been invoked to emphasize the role of preexisting rift-related structures on the location of intraplate earthquakes [*Crone et al*., 1985; *Thomas*, 2006, 2011; *Mazzotti*, 2007]. The similarity of the MSF with other structures of the NMSZ (e.g., the Cottonwood Grove Fault, [*Hamilton and Zoback*, 1982]) and its proximity to the eastern margin of the Reelfoot Rift suggests that the MSF might have formed during the early stages of rifting in Late Precambrian-Early Cambrian and then reactivated repeatedly throughout the tectonic history of the southern margin of Laurentia as the increasing amount of the deformation with age observed along the fault suggests. The interpretation of nearly vertically oriented faults such as the MSF as inherited from a failed rift structure however poses the problem of how these faults might have been generated in a rift environment, where one might expect steeply dipping normal faults rather than vertical structures. A plausible explanation is that the rift might have resulted from the right-lateral strike-slip motion along the northwestern oriented Paleozoic transform margin at the southern edge of Laurentia [*Thomas*, 1985, 2006]

[39] Presently, the kinematics of the left-lateral step over structure and the right-lateral strike-slip faults of the NMSZ fault system are explained as a restraining bend in the context of a right-lateral strike-slip system in a currently near east-west oriented compressional stress field [*Zoback and Zoback*, 1980; *Cunningham and Mann*, 2007; *Csontos et al*., 2008; *Tavakoli et al*., 2010; *Pratt*, 2012]. A restraining bend zone is frequently observed in a context of a complex shear faulting pattern in a strike-slip system, such as the Akato Tagh bend along the Altyn Tagh fault, the Big Bend along the San Andreas Fault, and the Yammuneh bend along the Dead Sea Fault [*Mann et al*., 1984; *Sylvester*, 1988; *Cowgill et al*., 2004]. Complex structures preferentially develop at these bending nodes rather than along the straight portion of the same fault and can be explained by the Riedel shear theory, a faulting mechanism of brittle crust applied to many other studies [*Sylvester*,

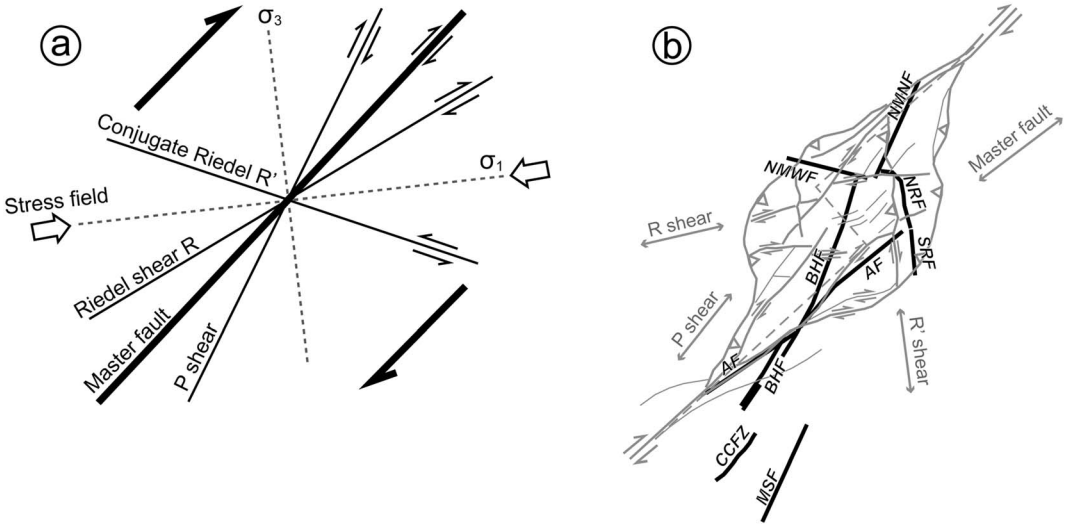

Figure 10. (a) Schematic figure of right-lateral Riedel shear, indicating the faulting pattern in the vicinity of the NMSZ. The regional compressional stress field is oriented about N80°E [*Zoback and Zoback*, 1980; *Grana and Richardson*, 1996], the master fault orientation is about N45°E [*Csontos and Van Arsdale*, 2008], the ideal *P* shear direction is about N30°E, and conjugate Riedel shear R′ about N70°W. In this system, the MSF is interpreted as a *P* shear fault. (b) Faulting pattern generated in a 90° natural step over sandbox model (light gray lines) [*McClay and Bonora*, 2001] and the main faults in the vicinity of the NMSZ (heavy black lines). The arrowed gray lines represent the generalized directions of the fractures in the sandbox experiment and their association with the Riedel shear pattern [after *Pratt*, 2012].

1988; *Crone et al*., 1995; *Katza et al*., 2004; *Coelho et al*., 2006; *Tavakoli et al*., 2010]. A series of sandbox analog modeling studies have been carried out to simulate the faulting pattern of strike-slip faults with step over features in compressional regimes [*Richard*, 1991; *Schreurs*, 1994; *McClay and Bonora*, 2001; *Pratt*, 2012]. Experimental results show that the main fractures follow orientations of the Riedel shear (R), the conjugate Riedel shear (R′), and the *P* shear fractures (Figure 10a).

[40] Results from a scaled sandbox analog model of a 90° neutral restraining step over experiment [*McClay and Bonora*, 2001] shows the fit between experimental ruptures and real faults in the vicinity of the NMSZ (Figure 10b). The Axial Fault (AF) and the New Madrid North Fault (NMNF) represent the main faults in the Riedel shear pattern. The New Madrid West Fault (NMWF) is consistent with the conjugate Riedel shear faults. The Bootheel Fault (BHF) fits the fracture of the *P* shear in the central part of the fractured region. Because both the BHF (N24°E) and the MSF (N25°E) trend in the same direction as the *P* shear fracture, we suggest that the MSF also is a *P* shear fault, controlled by the northeast-trending basement faults at the southeastern margin of the Reelfoot Rift and reactivated under the present east-northeast compressional stress field [*Howe and Thompson*, 1984; *Howe*, 1985; *Harrison and Schultz*, 2002; *Csontos et al*., 2008]. Additionally, we suggest that similarly to the BHF, which has been interpreted as the transfer fault between the AF and the NMNF during the Cenozoic [*Guccione et al*., 2005], the MSF might also extend further to the northeast along its strike to either the intersection of the AF with the Reelfoot Thrust faults or to the southeastern terminus of the Reelfoot Thrust, acting as a transfer fault between the Reelfoot Thrust and presently inactive faults to the south. The latter interpretation has implications for strain accommodation and seismicity of the South Reelfoot Fault (SRF), bounded by the dextral strike-slip AF and the MSF. This portion of the seismicity, interpreted as a restraining bend [*Csontos et al*., 2008], is southeast of the left-stepping right-lateral fault system defined by the NMNF and the AF [*Russ*, 1982; *Schweig and Van Arsdale*, 1996]. We suggest that the northeastward movement of the SRF might be associated with right-lateral displacement along the MSF and along the Eastern Reelfoot Rift Margin, as suggested by *Cox et al*. [2006].

6. Conclusions

[41] New high-resolution marine and land seismic reflection data were acquired in 2008, 2010, and 2011 to study the long-term deformation in the Mississippi Embayment outside the NMSZ. As part of this project, a total of five new seismic profiles imaged a ~45 km long fault, which we interpret as the southwestern continuation of the MSF, originally imaged by *Williams et al*. [2001]. The fault strikes N25°E, dips ~83° west-northwest, and exhibits an up-to-the-west sense of motion. The fault deforms the unconsolidated sediment in the embayment from the Paleozoic rocks up to the Quaternary alluvium, offsetting the top of the Paleozoic by an average of ~77 m and folding the top of the Cretaceous and the Paleocene sections by averages of ~44 and ~25 m, respectively. Additionally, the base of the Quaternary alluvium is folded consistently with the lower units, and the fold displays a maximum deformation of ~28 m on one profile. An eastward-dipping reverse fault, WMSF, is imaged in the profiles, forming an anticline together with the MSF. The anticline, as well as the two faults (MSF and WMSF) that bound it, could be the upper portion of a compressional strike-slip system (positive flower structure), which merges at deeper part, in light

of the N80°E compressional regional stress field [*Zoback and Zoback*, 1980; *Grana and Richardson*, 1996].

[42] The fault shows a consistent increase in the amount of deformation from the youngest to the oldest stratigraphic units on all seismic profiles suggesting prolonged activity of the fault throughout the Mesozoic and the Cenozoic. From northeast to southwest, the amount of deformation decreases along the fault, and the data suggest that this fault steps to the west in an en echelon pattern south of Memphis, Tennessee.

[43] Vertical slip rates calculated using fault parameters are 0.0022, 0.0010, 0.0004, and 0.2154 mm/yr for the Late Cretaceous, the Paleocene, the Eocene, and the Quaternary, respectively. These values are comparable with those calculated for structures associated with the active Reelfoot fault system [*Van Arsdale*, 2000] and corroborate the evidence for an increase in strain rates during the late Quaternary. However, the lack of age constraint at the base of the Quaternary section is a major source of uncertainty about the Quaternary activity of the fault.

[44] Source scaling estimates [*Wells and Coppersmith*, 1994] for the MSF indicate that the fault is capable of generating a *M*6.9 earthquake if rupturing in one event. The seismic potential of the MSF coupled with the evidence for an increase in fault activity during the late Quaternary as well as its proximity (only 9 km) to downtown Memphis suggest that the MSF could present a higher seismic threat to Memphis than the NMSZ itself.

[45] **Acknowledgments.** We thank Steffen Saustrup (UTIG) for his critical work in the operation and maintenance of the UTIG high-resolution marine seismic system. We thank Jack Odum and David Worley (USGS), IRIS intern Dylan Meyer, and CERI students (Leah Mitchell, Michael Towle, Salomon Ayele, Paul Ogwari, Shishay Bisrat, and Onur Mataracioglu), who helped with data acquisition. We thank the USACE (especially Tony Johnston and the crew of the M/V Strong) and NEES for supporting field operations. We also thank Randel T. Cox, Roy Van Arsdale, and Daniel Pryne for helpful discussions and comments. We thank Robert A. Williams, an anonymous reviewer, and the Editor Todd Ehlers for helping to improve this paper with their detailed comments. This research is funded by NSF-EAR award 0738853 and 0948619 to the University of Memphis, NSF-EAR awards 0738855 and 0948562 to the University of Texas, USGS NEHRP Awards 08HQGR0089 and 08HQGR0090 to the University of Memphis and University of Texas, respectively, and G10AP00012 to the University of Memphis.

References

Autin, W. J., S. F. Burns, B. J. Miller, R. T. Saucier, and J. I. Snead (1991), Quaternary geology of the Lower Mississippi Valley, in *The Geology of North America, Vol K-2, Quaternary Nonglacial Geology: Conterminous U.S.*, edited by R. B. Morrison, pp. 547–582, Geol. Soc. Am., Boulder, Colo.

Baldwin, J. N., J. B. Harris, R. B. Van Arsdale, R. Givle, K. I. Kelson, J. L. Sexton, and M. Lake (2005), Constraints on the location of the late Quaternary Reelfoot and New Madrid North Faults in the Northern New Madrid Seismic Zone, Central United States, *Seismol. Res. Lett.*, *76*(6), 772–789, doi:10.1785/gssrl.76.6.772.

Bexfield, C. E., J. H. McBride, A. J. M. Pugin, W. J. Nelson, T. H. Larson, and S. L. Sargent (2005), The Olmsted fault zone, southernmost Illinois: A key to understanding seismic hazard in the northern new Madrid Seismic Zone, *Eng. Geol.*, *81*, 179–201.

Bexfield, C. E., et al. (2006), Integration of *P*- and *SH*-wave high-resolution seismic reflection and micro-gravity techniques to improve interpretation of shallow subsurface structure: New Madrid Seismic Zone, *Tectonophysics*, *420*, 5–21.

Blum, M. D., M. J. Guccione, D. A. Wysocki, P. C. Robnett, and E. M. Rutledge (2000), Late Pleistocene evolution of the lower Mississippi River valley, southern Missouri to Arkansas, *Geol. Soc. Am. Bull.*, *112*(2), 221–235.

Braile, L. W., W. J. Hinze, G. R. Keller, E. G. Lidiak, and J. L. Sexton (1986), Tectonic development of the New Madrid rift complex, Mississippi Embayment, North America, *Tectonophysics*, *131*(1–2), 1–21, doi:10.1016/0040-1951(86)90265-9.

Broughton, A. T., R. B. Van Arsdale, and J. H. Broughton (2001), Liquefaction susceptibility mapping in the City of Memphis and Shelby County, Tennessee, *Eng. Geol.*, *62*, 207–222, doi:10.1016/S0013-7952(01)00062-X.

Burke, K. (1980), Intracontinental rifts and aulacogens, in *Continental Tectonics*, edited by B. C. Burchfiel, J. E. Oliver, and L. T. Silver, pp. 41–49, Natl. Acad. of Sci., Washington, D.C.

Calais, E., and S. Stein (2009), Time-variable deformation in the New Madrid Seismic Zone, *Science*, *323*, 1442, doi:10.1126/science.1168122.

Calais, E., J. Y. Han, C. DeMets, and J. M. Nocquet (2006), Deformation of the North American plate interior from a decade of continuous GPS measurements, *J. Geophys. Res.*, *111*, B06402, doi:10.1029/2005JB004253.

Calais, E., A. M. Freed, R. B. Van Arsdale, and S. Stein (2010), Triggering of New Madrid seismicity by late-Pleistocene erosion, *Nature*, *466*, doi:10.1038/nature09258.

Chen, H., J. Chiu, J. Pujol, K. Kim, K. Chen, B. Huang, Y. Yeh, and S. Chiu (2006), A simple algorithm for local earthquake location using 3D Vp and Vs models: Test examples in the Central United States and in Central Eastern Taiwan, *Bull. Seismol. Soc. Am.*, *96*(1), 288–305, doi:10.1785/0120040102

Chiu, J. M., A. C. Johnston, and Y. T. Yang (1992), Imaging the active faults of the central New Madrid Seismic Zone using PANDA array data, *Seismol. Res. Lett.*, *63*, 375–393.

Chiu, S., J. Chiu, and A. C. Johnston (1997), Seismicity of the southeastern margin of Reelfoot Rift, central United States, *Seismol. Res. Lett.*, *68*(5), 785–796, doi:10.1785/gssrl.68.5.785.

Coelho, S., C. Passchier, and F. Marques (2006), Riedel-shear control on the development of pennant veins: Field example and analogue modeling, *J. Struct. Geol.*, *28*(9), 1658–1669, doi:10.1016/j.jsg.2006.05.009.

Cowgill, E., Y. An, J. R. Arrowsmith, X. Wang, and S. Zhang (2004), The Akato Tagh bend along the Altyn Tagh fault, northwest Tibet 1: Smoothing by vertical-axis rotation and the effect of topographic stresses on bend-flanking faults, *Geol. Soc. Am. Bull.*, *116*(11–12), 1423–1442, doi:10.1130/B25359.1.

Cox, R. T., and R. B. Van Arsdale (1997), Hotspot origin of the Mississippi Embayment and its possible impact on contemporary seismicity, *Eng. Geol.*, *46*(3–4), 201–216, doi:10.1016/S0013-7952(97)00003-3.

Cox, R. T., and R. B. Van Arsdale (2002), The Mississippi Embayment, North America: A first order continental structure generated by the Cretaceous superplume mantle event, *J. Geodyn.*, *34*, 163–176.

Cox, R. T., J. Cherryhomes, J. B. Harris, D. Larsen, R. B. Van Arsdale, and S. L. Forman (2006), Paleoseismology of the southeastern Reelfoot Rift in western Tennessee and implications for intraplate fault zone evolution, *Tectonics*, *25*, TC3019, doi:10.1029/2005TC001829.

Cox, R. T., A. A. Hill, D. Larsen, T. L. Holzer, S. L. Forman, T. E. Noce, C. Gardner, and J. Morat (2007), Seismotectonic implications of sand blows in the southern Mississippi Embayment, *Eng. Geol.*, *89*, 278–299, doi:10.1016/j.enggeo.2006.11.002.

Cox, R. T., R. B. Van Arsdale, D. Clark, A. Hill, and D. Lumsden (2013), A revised paleo-earthquake chronology on the Southeast Reelfoot Rift margin near Memphis, Tennessee, *Seismol. Res. Lett.*, *84*(2), 402–408, doi:10.1785/0220120142.

Crone, A. J., F. A. McKeown, S. T. Harding, R. M. Hamilton, D. P. Russ, and M. D. Zoback (1985), Structure of the New Madrid seismic source zone in southeastern Missouri and northeastern Arkansas, *Geology*, *13*(8), 547–550.

Crone, A. J., M. Giardino, and E. S. Schweig III (1995), Paleoseismic studies of the Bootheel lineament, southeastern Missouri, and the Crittenden County fault zone, northeastern Arkansas, New Madrid Seismic Zone, central United States, *U. S. Geol. Surv. Miscellaneous Field Studies Map MF-2279*, 21.

Crone, A. J., P. M. De Martini, M. N. Machette, K. Okumura, and J. R. Prescott (2003), Paleoseismicity of two historically quiescent faults in Australia: Implications for fault behavior in stable continental regions, *Bull. Seismol. Soc. Am.*, *93*(5), 913–1934, doi:10.1785/0120000094.

Csontos, R., and R. B. Van Arsdale (2008), New Madrid Seismic Zone fault geometry, *Geosphere*, *4*(5), 802–813, doi:10.1130/GES00141.1.

Csontos, R., R. B. Van Arsdale, and B. Waldron (2008), Reelfoot Rift and its impact on Quaternary deformation in the central Mississippi River valley, *Geosphere*, *4*(1), 145–158.

Cunningham, W. D., and P. Mann (Eds.) (2007), Tectonics of Strike-Slip Restraining and Releasing Bends, *Spec. Publ. Geol. Soc. London*, *290*, 125, doi:10.1144/SP290.2.

Ervin, C. P., and L. D. McGinnis (1975), Reelfoot Rift: Reactivated precursor to the Mississippi Embayment, *Geol. Soc. Am. Bull.*, *86*, 1287–1295, doi:10.1130/0016-7606.

Fisk, H. N. (1944), *Geological Investigation of the Alluvial Valley of the Lower Mississippi River*, Miss. River Comm., U. S. Army Corps of Eng., Vicksburg, Miss.

Frankel, A., R. Smalley, and J. Paul (2012), Significant motions between GPS sites in the New Madrid Region: Implications for seismic hazard, *Bull. Seismol. Soc. Am.*, *102*(2), 479–489, doi:10.1785/0120100219.

Ge, J. (2009), Determination of shallow shear-wave attenuation in the Mississippi Embayment using vertical seismic profiling data, *Bull. Seismol. Soc. Am.*, *99*(3), 1636–1649.

Grana, J. P., and R. M. Richardson (1996), Tectonic stress within the New Madrid Seismic Zone, *J. Geophys. Res.*, *101*(B3), 5445–5458.

Guccione, M. J., R. Marple, and W. J. Autin (2005), Evidence for Holocene displacements on the Bootheel fault (lineament) in southeastern Missouri: Seismotectonic implications for the New Madrid region, *Geol. Soc. Am. Bull.*, *117*(3/4), 319–333, doi:10.1130/B25435.1.

Hamilton, R. M., and M. D. Zoback (1982), Tectonic features of the New Madrid seismic zone from seismic-reflection profiles, in *Investigations of the New Madrid, Missouri Earthquake Region*, edited by F. A. McKeown, and L. C. Pakiser, *U. S. Geol. Surv. Prof. Pap*., *1236*, 55–81.

Hardesty, K., L. W. Wolf, and P. Bodin (2010), Noise to signal: A microtremor study at liquefaction sites in the New Madrid Seismic Zone, *Geophysics*, *75*(3), B83–B90.

Harris, J. B. (2009), Hammer-impact *SH*-wave seismic reflection methods in neotectonic investigations: General observations and case histories from the Mississippi Embayment, USA, *J. Earth Sci.*, *20*(3), 513–525.

Harris, J. B., and J. L. Sorrells (2006), Shear-wave seismic reflection images of the Big Creek fault zone near Helena, Arkansas, SEG New Orleans 2006 Annual Meeting, SEG Technical Program Expanded Abstracts.

Harrison, R. W., and A. Schultz (2002), Tectonic framework of the southwestern margin of the Illinois Basin and its influence on neotectonism and seismicity, *Seismol. Res. Lett.*, *73*(5), 698–731, doi:10.1785/gssrl.73.5.698.

Hildenbrand, T. G., and J. D. Hendricks (1995), Geophysical setting of the Reelfoot Rift and relations between rift structures and the New Madrid Seismic Zone, *U.S. Geol. Surv. Prof. Pap. 1538-E*.

Hough, S. E., J. G. Armbruster, L. Seeber, and J. F. Hough (2000), On the modified Mercalli intensities and magnitudes of the 1811–1812 New Madrid earthquakes, *J. Geophys. Res.*, *105*(B10), 23,839–23,864, doi:10.1029/2000JB900110.

Howe, J. R. (1985), Tectonics, sedimentation, and hydrocarbon potential of the Reelfoot Aulocogen, MS Thesis, Univ. of Okla., Norman.

Howe, J. R., and T. L. Thompson (1984), Tectonics, sedimentation, and hydrocarbon potential of the Reelfoot Rift, *Oil Gas J.*, *82*, 179–190.

Johnston, A. C., and L. R. Kanter (1990), Earthquakes in stable continental crust, *Sci. Am.*, *262*(3), 68–75.

Johnston, A. C., and E. S. Schweig III (1996), The enigma of the New Madrid earthquakes of 1811–1812, *Annu. Rev. Earth Planet. Sci. Lett.*, *24*, 339–384.

Katza, Y., R. Weinberger, and A. Aydin (2004), Geometry and kinematic evolution of Riedel shear structures, Capitol Reef National Park, Utah, *J. Struct. Geol.*, *26*, 491–501, doi:10.1016/j.jsg.2003.08.003.

Langston, C. A. (2003), Local earthquake wave propagation through Mississippi Embayment sediments, Part I: Body-wave phases and local site responses, *Bull. Seismol. Soc. Am.*, *93*(6), 2664–2684.

Liu, M., S. Stein, and H. Wang (2011), 2000 years of migrating earthquakes in North China: How earthquakes in midcontinents differ from those at plate boundaries, *Lithosphere*, doi:10.1130/L129.1.

Luzietti, E. A., L. R. Kanter, E. S. Schweig III, K. M. Shedlock, and R. B. Van Arsdale (1995), Shallow deformation along the Crittenden Country Fault Zone near the southeastern margin of the Reelfoot Rift, Northeastern Arkansas, *U.S. Geol. Surv. Prof. Pap. 1538-J*.

Magnani, M. B., and K. McIntosh (2009), Toward an understanding of the long-term deformation in the Mississippi Embayment, *NEHRP Rep. 08HQGR0089/08HQGR0090*, Natl. Sci. Found, Washington, D.C.

Mann, P., K. Burke, and T. Matumoto (1984), Neotectonics of Hispaniola: Plate motion, sedimentation, and seismicity at a restraining bend, *Earth Planet. Sci. Lett.*, *70*, 311–324.

Mazzotti, S. (2007), Geodynamic models for earthquake studies in intraplate North America, *Geol. Soc. Am. Spec. Pap.*, *425*, 17–33, doi:10.1130/2007.2425(02).

McBride, J. H., W. J. Nelson, and W. J. Stephenson (2002), Integrated geological and geophysical study of Neogene and Quaternary-age deformation in the Northern Mississippi Embayment, *Seismol. Res. Lett.*, *73*(5), 597–627, doi:10.1785/gssrl.73.5.597.

McClay, K., and M. Bonora (2001), Analog models of restraining stepovers in strike-slip fault systems, *AAPG Bull.*, *85*(2), 233–260.

Meyer, D., M. B. Magnani, and K. McIntosh (2011), Erosion and deposition patterns of the Mississippi River as a result of "100-year" flood event of April 2011, AGU 2011 Fall Meeting poster, EP31D-0849.

Newman, A., S. Stein, J. Weber, J. Engeln, A. Mao, and T. Dixon (1999), Slow deformation and lower seismic hazard at the New Madrid Seismic Zone, *Science*, *284*(23), 619–621.

Nuttli, O. W. (1973), The Mississippi Valley earthquakes of 1811 and 1812: Intensities, ground motion, and magnitudes, *Bull. Seismol,. Soc. Am.*, *63*(1), 227–248.

Odum, J. K., W. J. Stephenson, K. M. Shedlock, and T. L. Pratt (1998), Near-surface structural model for deformation associated with the February 7, 1812, New Madrid, Missouri, earthquake, *Geol. Soc. Am. Bull.*, *110* (2), 149–162.

Odum, J. K., W. J. Stephenson, and R. A. Williams (2010), Multisource, high-resolution seismic-reflection imaging of Meeman-Shelby Fault and a possible tectonic model for a Joiner Ridge–Manila High Stepover Structure, *Seismol. Res. Lett.*, *81*(4), 647–663, doi:10.1785/gssrl.81.4.647.

Parrish, S., and R. B. Van Arsdale (2004), Faulting along the southeastern margin of the Reelfoot Rift in northwestern Tennessee revealed in deep seismic-reflection profiles, *Seismol. Res. Lett.*, *75*(6), 784–793, doi:10.1785/gssrl.75.6.784.

Pratt, T. L. (1994), How old is the New Madrid Seismic Zone? *Seismol. Res. Lett.*, *65*(2), 172–179.

Pratt, T. L. (2012), Kinematics of the New Madrid Seismic Zone, central United States, based on stepover models, *Geology*, *40*(4), 371–374, doi:10.1130/G32624.1.

Richard, P. (1991), Experiments on faulting in a two-layer cover sequence overlying a reactivated basement fault with oblique-slip, *J. Struct. Geol.*, *13*(4), 459–469.

Rittenour, T. M., M. D. Blum, and R. J. Goble (2007), Fluvial evolution of the lower Mississippi River valley during the last 100 k.y. glacial cycle: Response to glaciation and sea-level change, *Geol. Soc. Am. Bull.*, *119*(5–6), 586–608.

Russ, D. P. (1982), Style and significance of surface deformation in the vicinity of New Madrid, Missouri, in *Investigations of the New Madrid, Missouri, Earthquake Region*, edited by F. A. McKeown, and L. C. Pakiser, *U. S. Geol. Surv. Prof. Pap*, *1236*, 95–114.

Saucier, R. T. (1994), *Geomorphology and Quaternary Geologic History of the Lower Mississippi Valley*, Waterways Exper. Station, U. S. Army Corps of Eng., Vicksburg, Miss.

Schreurs, G. (1994), Experiments on strike-slip faulting and block rotation, *Geology*, *22*, 567–570.

Schweig, E. S., III, and R. T. Marple (1991), The Bootheel lineament: A possible coseismic fault of the great New Madrid earthquakes, *Geology*, *19*, 1025–1028.

Schweig, E. S., III, and R. B. Van Arsdale (1996), Neotectonics of the upper Mississippi Embayment, *Eng. Geol.*, *45*, 185–203.

Shedlock, K. M., and S. T. Harding (1982), Mississippi River seismic survey, *Geophys. Res. Lett.*, *9*(11), 1275–1278.

Stearns, R. G. (1957), Cretaceous, Paleocene, and lower Eocene: Geologic history of the northern Mississippi Embayment, *Geol. Soc. Am. Bull.*, *68*(9), 1077–1100, doi:10.1130/0016-7606.

Stein, S. (2007), Approaches to continental intraplate earthquake issues, continental intraplate earthquakes: Science, hazard, and policy issues, *Geol. Soc. Am. Spec. Pap.*, *425*, 1–16.

Stein, S., and A. Newman (2004), Characteristic and uncharacteristic earthquakes as possible artifacts: Application to the New Madrid and Wabash Seismic Zone, *Seismol. Res. Lett.*, *75*, 173–187.

Stein, S., M. Liu, E. Calais, and Q. Li (2009), Mid-continent earthquakes as a complex system, *Seismol. Res. Lett.*, *80*(4), 551–553, doi:10.1785/gssrl.80.4.551.

Stephenson, W. J., K. M. Shedlock, and J. K. Odum (1995), Characterization of the Cottonwood Grove and Ridgely Faults near Reelfoot Lake, Tennessee, from high-resolution seismic reflection data, *U.S. Geol. Surv. Prof. Pap. 1538-I*.

Sylvester, A. G. (1988), Strike-slip faults, *Geol. Soc. Am. Bull.*, *100*(11), 1666–1703, doi:10.1130/0016-7606(1988)100 < 1666:SSF > 2.3.CO;2.

Tavakoli, B., S. Pezeshk, and R. T. Cox (2010), Seismicity of the New Madrid Seismic Zone derived from a deep-seated strike-slip fault, *Bull. Seismol. Soc. Am.*, *100*(4), 1646–1658, doi:10.1785/0120090220.

Thomas, W. A. (1985), The Appalachian-Ouachita connection: Paleozoic orogenic belt at the southern margin of North America, *Annu. Rev. Earth Planet. Sci.*, *13*, 175–199, doi:10.1146/annurev.ea.13.050185.001135.

Thomas, W. A. (1991), The Appalachian-Ouachita rifted margin of southeastern North America, *Geol. Soc. Am. Bull.*, *103*(3), 415–431.

Thomas, W. A. (2006), Tectonic inheritance at a continental margin, *Geol. Soc. Am. Today*, *16*(2), 4–11, doi:10.1130/1052-5173(2006)016[4:TIAACM]2.0.CO;2.

Thomas, W. A. (2010), Interactions between the southern Appalachian–Ouachita orogenic belt and basement faults in the orogenic footwall and foreland, *Geol. Soc. Am. Mem.*, *206*, 897–916, doi:10.1130/2010.1206(34).

Thomas, W. A. (2011), The Iapetan rifted margin of southern Laurentia, *Geosphere*, *7*, 97–120, doi:10.1130/GES00574.1.

Tuttle, M. P., E. S. Schweig, J. D. Sims, R. H. Lafferty, L. W. Wolf, and M. L. Haynes (2002), The earthquake potential of the New Madrid Seismic Zone, *Bull. Seismol. Soc. Am.*, *92*(6), 2080–2089.

Tuttle, M. P., H. Al-Shukri, and H. Mahdi (2006), Very large earthquakes centered southwest of the New Madrid Seismic Zone 5000–7000 years ago, *Seismol. Res. Lett.*, *77*(6), 755–770.

Van Arsdale, R. B. (2000), Displacement history and slip rate on the Reelfoot fault of the New Madrid seismic zone, *Eng. Geol.*, *55*, 219–226.

Van Arsdale, R. B. (2009), Adventures through deep time: The Central Mississippi River Valley and its earthquakes, *Geol. Soc. Am. Spec. Pap. 455*.

Van Arsdale, R. B., and M. Ellis (2004), Characterization of active faults in the New Madrid Seismic Zone, *Mid-America Earthquake Cent. Rep., 04-02*.

Van Arsdale, R. B., R. Bresnahan, N. McCallister, and B. Waldron (2007), Upland Complex of the central Mississippi River valley: Its origin, denudation, and possible role in reactivation of the New Madrid seismic zone, *Continental Intraplate Earthquakes: Science, Hazard, and Policy Issues*, edited by S. Stein and S. Mazzotti, *Geol. Soc. Am. Spec. Pap., 425*, 177–192, doi:10.1130/2007.2425(13).

Velasco, M., R. B. Van Arsdale, B. Waldron, J. B. Harris, and R. T. Cox (2005), Quaternary faulting beneath Memphis, Tennessee, *Seismol. Res. Lett.*, *75*(5), 598–614.

Vidale, J., et al. (2011), Independent expert panel on New Madrid Seismic Zone earthquake hazards, NMSZ Expert Panel Report to NEPEC, April 16, 2011.

Wells, D. L., and K. J. Coppersmith (1994), New empirical relationships among magnitude, rupture length, rupture width, rupture area, and surface displacement, *Bull. Seismol. Soc. Am.*, *84*(4), 974–1002.

Williams, R. A., E. A. Luzietti, and D. L. Carver (1995), High-resolution seismic imaging of Quaternary faulting on the Crittenden County fault zone, New Madrid Seismic Zone, Northeastern Arkansas, *Seismol. Res. Lett.*, *66*(3), 42–57, doi:10.1785/gssrl.66.3.42.

Williams, R. A., W. J. Stephenson, J. K. Odum, and D. M. Worley (2001), Seismic-reflection imaging of Tertiary faulting and related post-Eocene deformation 20 km north of Memphis, Tennessee, *Eng. Geol.*, *62*(1–3), 79–90.

Zoback, M. L., and M. Zoback (1980), State of stress in the conterminous United States, *J. Geophys. Res.*, *85*(B11), 6113–6156.